

A fuzzy rule based approach to cloud cover estimation

A. Ghosh*, N.R. Pal, J. Das

Electronics and Communication Sciences Unit, Indian Statistical Institute, 203, B.T. Road, Calcutta, 700108, India

Received 17 January 2005; received in revised form 20 November 2005; accepted 20 November 2005

Abstract

A fuzzy rule based cloud classification scheme is proposed to estimate the cloud cover from satellite imagery. METEOSAT-5 images are classified into three classes: cloudy, partially cloudy, and clear sky. Five features, which measure the temporal and spatial properties of visible (VIS) and infrared (IR) images of METEOSAT-5, are used for this. The proposed classifier finds out a few human understandable rules (fuzzy rules) using exploratory data analysis. A novel attribute of the system is that it analyzes the behavior of misclassifications during training (i.e., typical mistakes) to extract a few more rules which are augmented to the initial rule base to improve its performance. The scheme is tested on images other than the training image(s) and the performance is found to be quite satisfactory. A post-processing scheme is also developed, which utilizes experts' knowledge to generate additional rules to account for coastal region, sunglint areas, and snow-covered Himalayan region. This improves the performance of the system further. Finally, the classification results are compared with multispectral threshold tests, surface synoptic observations, and total cloud cover (tcdc) of reanalysis data produced by National Centers for Environmental Prediction (NCEP) and National Center for Atmospheric Research (NCAR). The high accuracy achieved by the proposed method may be attributed to (1) better design philosophy of classifiers; (2) good choice for the feature vectors; (3) accurate labeling of training data; and (4) exploitation of experts' knowledge.

Keywords: Fuzzy rule base; Classification; Typical mistake; Post-processing; False firing; Cloud cover; METEOSAT-5

1. Introduction

Clouds cover roughly half of the Earth. Clouds constitute major factors in determining the radiation budget of the Earth, and they play crucial, and as yet not completely understood, roles in modulating the climate (Norris, 2000; Wielicki et al., 1995). Space-based instruments are the only means by which the global distribution of clouds can be adequately sampled. Many satellite image based studies have focused on obtaining knowledge of the characteristics and distribution of clouds and their influence on the Earth's climate. This information has been primarily used by numerical climate modeling community. The crucial issues in this regard are automatic and accurate cloud identification from satellite images. The importance of this lies in the fact that a huge amount of image data, e.g., 1.8 GB/day from METEOSAT-5, are generated everyday. Extracting cloud field information from these images using visual/manual interpretation is a tedious and unreliable

task and moreover the results are, to some extent, operator dependent. Therefore, efficient and robust cloud classification schemes are needed for automatic processing of satellite cloud imagery for climatological applications.

In the recent years, considerable research has been focused on the cloud classification area. A rich history of cloud classification approaches was outlined by Hughes (1984), Goodman and Henderson-Sellers (1988), Rossow (1989) and Kidder and Velder Haar (1995). Most of the available satellite cloud cover estimation algorithms use some threshold mechanism (Connell et al., 2001; Reinke et al., 1992) or some other conventional statistical methods for separating cloudy pixels from cloud free ones (Coakley & Bretherton, 1982; Coakley & Baldwin, 1984; Desbois et al., 1981; Ebert, 1987, 1989; Pairman & Kittler, 1986; Pankiewicz, 1995; Rossow et al., 1985; Seze & Desbois, 1987; Seze & Pawloska, 2001). But unfortunately these methods often suffer due to the dependence of the images on surface properties; the situation becomes more complex due to the presence of partially or broken/mixed cloud covered pixels. Consequently, the selection of an appropriate set of thresholds becomes difficult (Kidder & Velder Haar, 1995). Since the partially cloud covered pixels are not

acknowledged by these methods the total coverage depends upon the threshold. If the threshold value is set higher/lower, less/more partially covered pixels are counted as cloudy/clear sky pixels. Several clustering methods, such as Dynamic clustering method (Desbois et al., 1981) and the Asymmetric Gaussian method (Simmer et al., 1982), are also used for identifying clouds in satellite images. These clustering methods being unsupervised, may not (usually will not) give the desired partitioning of the data. In a supervised mode, since we can use experts' knowledge to label the training data, we are likely to get better estimates. In the recent years, artificial intelligence tools are increasingly being used for classification. Different artificial intelligent approaches for cloud classification are outlined by Tovinkere et al. (1993). Neural network (Lee et al., 1990) and fuzzy expert system (Baum et al., 1995; 1997, Key et al., 1989; Tovinkere et al., 1993) have also been used for classification of geophysical data.

The present study takes a very different approach, demonstrating the application of fuzzy rule based classifiers to cloud cover estimation from METEOSAT-5 imageries. The problem is defined with three classes: cloudy, partially cloudy and clear sky. Owing to the fact that the partially cloudy class, which is neither purely cloudy nor purely clear (e.g., thin cirrus, some sub-pixel cumulus, thin clouds at the edge of a cloud system, etc.), overlaps with both cloudy and clear sky classes, the situation becomes quite complex. The present approach makes use of the ability of fuzzy rule based system to classify data in a complex decision space. The problem is addressed in the following ways: (1) experts (meteorologists) label some pixels for these three classes and features are computed from the images obtained by the VIS and IR channels of METEOSAT-5. (2) A supervised scheme for identifying a set of fuzzy rules using the training data is then developed. (3) The misclassifications during training are analyzed and few more rules are extracted for modeling the *typical mistakes*. These rules are then augmented to the initial rule base to improve its performance. (4) To further improve the classifier accuracy, a post-processing scheme is designed which utilize the "*false firing*" information detected by experts on examining the classified (test) image(s). *The system enhances its performance from its mistakes (typical mistakes and false firing)*, this is a unique characteristic of the proposed system. (5) The scheme is finally applied on a set of test images and the results are visually compared with the multispectral threshold tests, surface synoptic observations, and NCEP/NCAR reanalysis "tcdc" data (Kalnay et al., 1996). Results show that proposed fuzzy system detects cloudy, partially cloudy, and clear sky classes with high accuracy (96–99%). Consideration of partially cloudy pixels reduces the threshold dependent overestimate/underestimate of cloudy pixels.

The next section outlines the proposed classification methodology. The data used in this study are described in Section 3, results (without post-processing) are discussed in Section 4, the post-processing scheme and corresponding results are presented in Section 5, comparison with the multispectral threshold tests, surface synoptic observations,

and NCEP/NCAR reanalyzed 'tcdc' data is discussed in Section 6 and the conclusions are given in Section 7.

2. Proposed methodology: fuzzy rule based approach

The fuzzy logic approach, a different conceptual model to classify objects, is based on approximate reasoning. The fuzzy set theoretic framework provides a degree of support to each of the potential classes. A set of fuzzy rules is used to define (describe) the class label of each data point. The rules are defined on some attributes which are computed for each pixel. After the rule base is obtained, for every pixel, the attributes are computed and the degree of match of these attributes with each fuzzy rule is computed. The class label associated with the rule having the strongest match defines the class of the pixel.

The complete methodology consists of six steps: collection of samples or training data for each class (discussed in Section 2.1), computation of features that can discriminate between classes (discussed in Section 2.2), generation of a fuzzy rule base (discussed in Section 2.3), refining (tuning and pruning) of the rule base (discussed in Section 2.4), finding ambiguous decisions (discussed in Section 2.5), and finally adding extra rules to model the typical misclassifications (discussed in Section 2.6).

2.1. Deciding on training data set

Given a set of N images, we select a set of n images. From each of these n images we identify a set of patches corresponding to cloudy, partially cloudy, and clear sky. We consider only a few patches where we are confident about their types. In other words, we pick up a few areas which are definitely cloudy, some areas which definitely belong to clear sky and a few areas corresponding to partially cloudy sky. We acknowledge the fact that there could be different extents of partially cloudy conditions. In the training sample we include only pixels for which we do not have any doubt. Deviation from this will produce a graceful degradation in the rule firing strength and even then we should be able to detect partially cloudy condition. While selecting training samples, we carefully excluded sunglint areas and coastal region. Later, we analyze the performance of the system on such areas too and propose corrective actions. We have $N=31$ images and we select only $n=1$ image. Each of these images is of size 2300×1900 . Table 1 shows the number of pixels considered for designing and testing the system. However, more images can be used to generate the training data set and this is likely to improve further the performance of the system. Here our

Table 1
Distribution of labeled data for land and water

| Class | No. of pixels | |
|------------------|---------------|------------|
| | Over land | Over Water |
| Cloudy | 23,884 | 65,490 |
| Partially cloudy | 25,339 | 81,417 |
| Clear sky | 52,447 | 80,012 |
| Total | 101,670 | 226,919 |

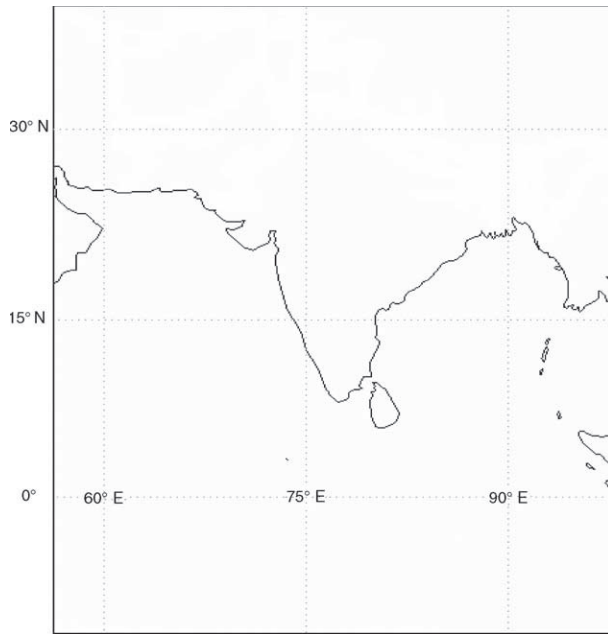


Fig. 1. The region of study: Indian subcontinent and Indian Ocean.

objective is to demonstrate the effectiveness of our system, so we restrict ourselves to a small data set.

2.2. Extraction of features

A set of features is extracted for each pixel taking into account its *temporal* as well as *spatial* context (Seze & Desbois, 1987). Here we use five features; three features are from the VIS channel image: mean, standard deviation, and mean difference from the cloud free background calculated using a 3×3 window around each pixel, and two features from the IR channel images: mean and standard deviation of brightness temperature calcu-

lated using a 3×3 window around each pixel. The third feature represents the temporal properties while the rest are associated with the spatial properties of the VIS count and IR brightness temperature data. In order to get the cloud free background image, we find the second darkest gray value at every pixel location over a large number of VIS channel images taken at a particular hour at least for a period of 1 month (discussed in Section 3.2).

2.3. Generation of the fuzzy rule base

Generation of an initial fuzzy rule base is done using exploratory data analysis. In particular, we use the k -means clustering algorithm to find a few clusters in the data corresponding to each class *separately*. Let $X = X_1 \cup X_2 \cup X_3$, $X_q \cap X_r = \Phi$, $r \neq q = 1, 2, 3$ be the training data, X_q be the training data corresponding to class q . Here the three classes are cloudy ($q=1$), partially cloudy ($q=2$), and clear sky ($q=3$). We cluster each $X_q \subseteq R^p$ using the k -means algorithm. Each cluster represents a dense/important area in the input space. Each such cluster is converted into a fuzzy rule of the form: if \mathbf{x} is CLOSE TO \mathbf{v} then the pixel is cloudy. Here \mathbf{x} is a feature vector in p -dimension and \mathbf{v} is the centroid of a cluster obtained from the data corresponding to the cloudy class. The fuzzy set CLOSE TO \mathbf{v} is represented by a set of p simpler atomic clauses: x_1 is CLOSE TO v_1 and x_2 is CLOSE TO v_2 and ... and x_p is CLOSE TO v_p . Here $\mathbf{v} = (v_1, v_2, \dots, v_p)^T$ and $\mathbf{x} = (x_1, x_2, \dots, x_p)^T$. In this way we get a set of initial rules. In general, the i th rule representing one of the c classes takes the form: x_1 CLOSE TO v_{i1} and ... and x_p CLOSE TO v_{ip} then the class is h . Here p is the number of features and hence the number of atomic clauses. The fuzzy set CLOSE TO v_{ij} is modeled by a Gaussian membership function: $\mu_{ij}(x_j; v_{ij}, \sigma_{ij}) = \exp(-(x_j - v_{ij})^2 / \sigma_{ij}^2)$, although, other choices are possible.

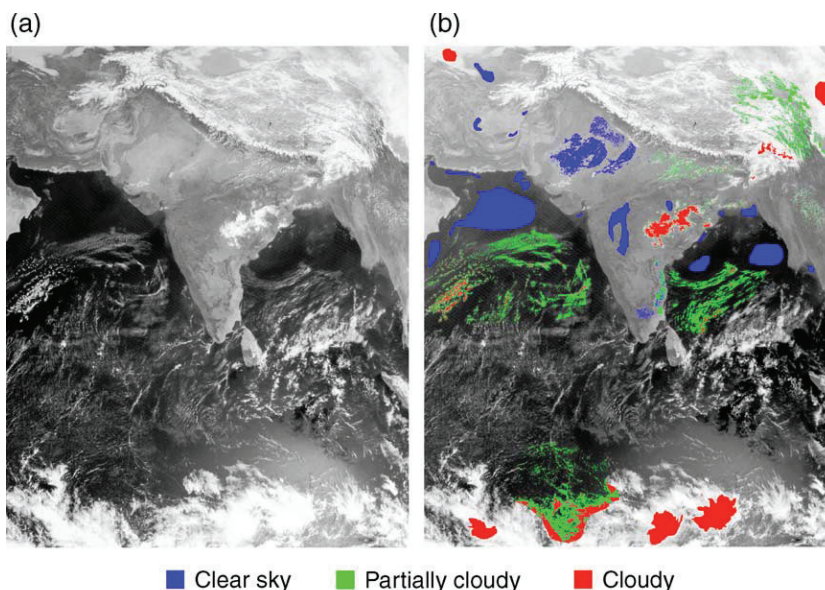


Fig. 2. METEOSAT-5 VIS ($0.5\text{--}0.9 \mu\text{m}$) image for the Indian subcontinent and in surrounding Indian Ocean, 0500 UTC 9th February 2003 (©2003 EUMETSAT); (a) histogram equalized image and (b) samples of cloudy, partially cloudy and clear sky classes labeled by meteorologists. The labeled data are summarized in Table 1.

Table 2
Initial fuzzy rule base over land surface

| Class | Rule no. | Feature no. | | | | | | | | | |
|------------------|----------|-------------|--------|----------|--------|----------|--------|----------|--------|----------|--------|
| | | 1 | | 2 | | 3 | | 4 | | 5 | |
| | | Centroid | Spread | Centroid | Spread | Centroid | Spread | Centroid | Spread | Centroid | Spread |
| Cloudy | 1 | 174.76 | 11.18 | 5.04 | 2.72 | 122.64 | 11.60 | 225.41 | 8.79 | 1.56 | 1.06 |
| | 2 | 151.73 | 10.17 | 9.59 | 5.25 | 109.71 | 10.45 | 257.63 | 12.49 | 1.17 | 0.97 |
| | 3 | 143.69 | 7.74 | 2.34 | 1.62 | 71.32 | 6.28 | 267.94 | 3.87 | 0.28 | 0.17 |
| | 4 | 120.51 | 10.17 | 13.11 | 6.16 | 82.80 | 9.51 | 264.61 | 10.02 | 1.70 | 1.41 |
| | 5 | 181.99 | 11.78 | 7.24 | 3.82 | 143.87 | 12.11 | 256.73 | 8.42 | 0.97 | 0.81 |
| Partially cloudy | 6 | 71.74 | 5.89 | 8.70 | 4.35 | 25.75 | 6.03 | 264.82 | 6.08 | 2.82 | 1.74 |
| | 7 | 84.05 | 5.34 | 6.01 | 3.30 | 28.27 | 6.38 | 253.28 | 7.32 | 2.32 | 1.49 |
| | 8 | 57.45 | 5.39 | 8.73 | 4.22 | 19.37 | 4.58 | 273.29 | 4.92 | 2.71 | 1.72 |
| | 9 | 53.76 | 4.05 | 4.27 | 2.58 | 14.13 | 3.06 | 286.55 | 5.59 | 1.27 | 1.21 |
| Clear sky | 10 | 63.23 | 5.24 | 1.23 | 0.74 | 6.89 | 3.71 | 288.36 | 5.03 | 0.26 | 0.18 |
| | 11 | 38.35 | 2.51 | 0.96 | 0.46 | 1.49 | 1.40 | 298.70 | 2.72 | 0.38 | 0.26 |
| | 12 | 82.63 | 6.49 | 2.63 | 1.68 | 20.17 | 5.38 | 279.03 | 2.21 | 0.46 | 0.29 |

Let there be M rules. So there will be M membership functions for each feature. We propose a simple, yet effective scheme to initialize the spread σ_{ij} of the Gaussian functions. From training data for each feature ($j=1, 2, \dots, p$) the maximum (\max_j) and minimum (\min_j) values are calculated. Within the interval $[\max_j, \min_j]$, v_{ij} s are then arranged in increasing order. Here v_{ij} s are the j th component of the cluster centers. Let the ordered values be $v_{i1,j}, v_{i2,j}, \dots, v_{iM,j}$ and the maximum and minimum values are $v_{i0,j} = \min_j$ and $v_{iM+1,j} = \max_j$, respectively. The k th membership function, $k=1, 2, \dots, M$, on the j th feature will have the center $v_{ik,j}$ and its spread is taken as:

$$\sigma_{ik,j} = \frac{1}{3} \max \{ (v_{ik+1,j} - v_{ik,j}), (v_{ik,j} - v_{ik-1,j}) \}.$$

Since the response of a Gaussian membership function beyond $\pm 3\sigma$ is negligible, we divide by 3. This choice will ensure sufficient overlaps with adjacent membership functions. In this way the initial rule base is defined. Sometimes this initialization may have a problem. It may take large values for the spreads, particularly at the class boundaries where the difference ($v_{ik+1,j} - v_{ik,j}$) may be large. To overcome this problem, for each feature ($j=1, 2, \dots, p$) the spread can be

initialized with the standard deviation (S.D.) of the j th components of the training data included in the associated cluster. This is just the initial choice. Since, the spreads are tuned, either initialization would be fine.

For a given data point \mathbf{x} , we first find the firing strength of each rule using the product T -norm (Klir & Yuan, 2001):

$$\alpha_i(\mathbf{x}) = \prod_{j=1}^{j=p} \mu_{ij}(x_j : v_{ij}, \sigma_{ij}).$$

Here $\alpha_i(\mathbf{x})$ is the firing strength of the i th rule on a data point \mathbf{x} . This gives the degree of match between the data point \mathbf{x} and the antecedent of the i th rule. Now class label of the rule having the maximum firing strength determines the class of the data point \mathbf{x} . Let $l = \underset{i}{\operatorname{argmax}} \alpha_i(\mathbf{x})$, and suppose the l th rule represents class c , then \mathbf{x} is assigned to class c .

2.4. Tuning and pruning of the rule base

2.4.1. Tuning of rule base

We now refine the rules to minimize the training error using gradient descent technique. Let $\mathbf{x} \in X$ be from the class c and R_c be the rule from class c giving the maximum firing strength

Table 3
Initial fuzzy rule base over water surface

| Class | Rule no. | Feature no. | | | | | | | | | |
|------------------|----------|-------------|--------|----------|--------|----------|--------|----------|--------|----------|--------|
| | | 1 | | 2 | | 3 | | 4 | | 5 | |
| | | Centroid | Spread | Centroid | Spread | Centroid | Spread | Centroid | Spread | Centroid | Spread |
| Cloudy | 1 | 160.84 | 12.92 | 5.94 | 4.82 | 135.39 | 10.04 | 232.35 | 16.34 | 1.54 | 1.11 |
| | 2 | 214.70 | 8.74 | 3.77 | 2.94 | 187.13 | 7.52 | 209.74 | 5.79 | 1.06 | 0.79 |
| | 3 | 189.15 | 8.60 | 4.16 | 3.12 | 161.82 | 8.88 | 218.47 | 7.07 | 1.23 | 0.84 |
| | 4 | 105.88 | 13.03 | 13.51 | 7.80 | 89.88 | 13.05 | 266.36 | 16.38 | 2.09 | 2.21 |
| | 5 | 67.75 | 10.90 | 12.48 | 6.94 | 51.85 | 10.36 | 274.05 | 13.71 | 1.88 | 1.73 |
| Partially cloudy | 6 | 24.20 | 2.26 | 2.77 | 1.51 | 8.73 | 2.01 | 290.14 | 2.60 | 0.36 | 0.42 |
| | 7 | 29.03 | 3.32 | 3.52 | 1.90 | 14.11 | 3.37 | 277.41 | 4.18 | 2.13 | 1.27 |
| | 8 | 43.30 | 5.36 | 14.40 | 6.09 | 25.76 | 4.89 | 288.63 | 2.59 | 0.96 | 0.57 |
| | 9 | 32.36 | 2.89 | 6.15 | 2.99 | 15.86 | 2.62 | 290.64 | 1.80 | 0.43 | 0.35 |
| Clear sky | 10 | 15.39 | 0.63 | 0.73 | 0.33 | -0.12 | 0.54 | 292.24 | 0.54 | 0.16 | 0.12 |
| | 11 | 26.36 | 2.54 | 0.81 | 0.38 | 4.72 | 1.62 | 289.79 | 0.87 | 0.16 | 0.12 |
| | 12 | 20.93 | 1.15 | 0.79 | 0.39 | 2.05 | 0.86 | 291.60 | 0.75 | 0.15 | 0.12 |

Table 4
Refined fuzzy rule base for land surface

| Class | Rule no. | Feature no. | | | | | | | | | |
|------------------|----------|-------------|--------|----------|--------|----------|--------|----------|--------|----------|--------|
| | | 1 | | 2 | | 3 | | 4 | | 5 | |
| | | Centroid | Spread | Centroid | Spread | Centroid | Spread | Centroid | Spread | Centroid | Spread |
| Cloudy | 1 | 175.21 | 15.56 | 4.91 | 7.94 | 123.82 | 15.70 | 225.19 | 14.37 | 1.62 | 5.31 |
| | 2 | 150.25 | 14.07 | 10.08 | 10.24 | 112.23 | 14.21 | 263.24 | 14.80 | 0.90 | 3.90 |
| | 3 | 143.36 | 10.28 | 2.19 | 5.16 | 72.20 | 10.97 | 268.70 | 5.20 | 0.28 | 1.88 |
| | 4 | 124.02 | 14.14 | 12.54 | 11.14 | 86.86 | 13.70 | 266.77 | 13.12 | 1.30 | 4.49 |
| | 5 | 176.02 | 14.68 | 6.79 | 8.44 | 138.71 | 15.41 | 259.62 | 12.22 | 0.72 | 3.37 |
| Partially cloudy | 6 | 67.16 | 13.98 | 9.66 | 11.20 | 25.51 | 13.03 | 265.88 | 13.05 | 2.91 | 6.93 |
| | 7 | 83.45 | 12.34 | 6.02 | 9.61 | 27.39 | 13.37 | 254.59 | 15.30 | 2.36 | 6.77 |
| | 8 | 53.35 | 11.49 | 7.37 | 10.21 | 16.89 | 9.90 | 277.30 | 12.55 | 2.65 | 7.11 |
| | 9 | 54.46 | 7.29 | 3.14 | 4.92 | 16.22 | 6.02 | 293.13 | 7.29 | 0.36 | 2.49 |
| Clear sky | 10 | 63.95 | 16.06 | 1.03 | 4.44 | 6.14 | 13.15 | 287.41 | 15.91 | 0.23 | 0.98 |
| | 11 | 38.07 | 7.43 | 0.96 | 3.66 | 1.41 | 4.89 | 298.21 | 9.10 | 0.39 | 2.82 |
| | 12 | 85.47 | 9.01 | 2.20 | 4.14 | 22.32 | 8.02 | 279.07 | 5.47 | 0.45 | 2.02 |

α_c for x . Also let R_{-c} be the rule from the incorrect classes having the maximum firing strength α_{-c} for x . We use an error function E .

$$E = \sum_{x \in X} (1 - \alpha_c + \alpha_{-c})^2.$$

This error function has been used by Chiu (1994) in the context of designing a fuzzy rule based classifier. The rules are refined by minimizing E with respect to the centroids and spreads associated with R_c and R_{-c} . This may be viewed as refining the rules with respect to their contexts in the feature space. The details of the rule refinement algorithm are given in the Appendix.

2.4.2. Pruning of bad rules

At the end of the rule base tuning we get the refined rule base which is expected to give a low error rate. Since we have derived these rules from the training data, without using any expert knowledge, there may be some poor rules which should be pruned out of the rule base. We consider two kinds of bad rules: rules not adequately represented by training data and rules that make more wrong decisions. A rule is said to be bad if it is fired only for a few training data points (here, if it is fired for ≤ 3 times). A rule is also bad if it makes more misclassifications than the number of correct classification.

2.5. Finding ambiguous decisions

We make a decision whether a pixel represents cloudy, partially cloudy or clear sky condition depending on the firing

strengths of the rules. The rule with the maximum firing strength is assumed to make the correct decision. For both land and water surface most of the correct decisions ($>96\%$, in some cases it is about 99%) are made with high firing strength, whereas in a few cases the maximum rule-firing strengths are very low (on the order of 10^{-14}). These low firing strength decisions may or may not be correct, one cannot be sure. So a threshold on the firing strength is defined for finding such ambiguous or weak decisions. Suppose a rule has p atomic clauses in its antecedent. Each atomic clause is modeled by a Gaussian membership function. Let $\sigma_i, i=1, 2, \dots, p$, be the spread of the Gaussian involved in a rule. For a Gaussian function 96% of the area under the curve lies between $\text{mean} \pm 2\sigma_i$. So the membership values beyond $\pm 2\sigma_i$ would be negligibly small. The membership value at $\pm 2\sigma_i$ is $\mu_{th} = e^{-4} = 1.8315639 \times 10^{-2}$. If an atomic clause is not satisfied at least to the extent μ_{th} , definitely that clause is very weakly satisfied. If none of the atomic clauses is satisfied at least to the extent μ_{th} , then the firing strength of that rule would be less than α_{thres} where α_{thres} is the result obtained by applying the T -norm on a set of p values each equal to μ_{th} . If we use min as the T -norm, then $\alpha_{thres} = \mu_{th}$. On the other hand, if we use product as the T -norm then $\alpha_{thres} = (\mu_{th})^p$. We shall call a decision ambiguous or weak, if the firing strength of the rule making the decision is less than α_{thres} .

2.6. Adding extra rules for typical mistakes

We start with 5 rules for cloudy class, 4 rules for partially cloudy class, and 3 rules for clear sky class, i.e., we begin with

Table 5
Classification results over land

| Class | Correct classification (%) | | | |
|------------------|----------------------------|---------|----------|---------|
| | Set 1 | | Set 2 | |
| | Training | Testing | Training | Testing |
| Cloudy | 99.73 | 99.82 | 98.37 | 98.56 |
| Partially cloudy | 98.3 | 98.25 | 97.22 | 98.43 |
| Clear sky | 97.93 | 99.02 | 96.87 | 97.1 |
| Overall | 98.65 | 99.01 | 97.48 | 97.75 |

Table 6
Classification results over water

| Class | Correct classification (%) | | | |
|------------------|----------------------------|---------|----------|---------|
| | Set 1 | | Set 2 | |
| | Training | Testing | Training | Testing |
| Cloudy | 99.43 | 99.27 | 98.71 | 98.69 |
| Partially cloudy | 97.6 | 97.67 | 97.1 | 97.33 |
| Clear sky | 99.2 | 99.74 | 98.63 | 99.01 |
| Overall | 98.74 | 98.86 | 98.15 | 98.42 |

Table 7
Confusion matrix on the training data over land

| Class | Cloudy | Partially cloudy | Clear sky |
|------------------|--------|------------------|-----------|
| Cloudy | 99.73 | 0.27 | 0.0 |
| Partially cloudy | 0.0 | 98.3 | 1.7 |
| Clear sky | 0.0 | 2.07 | 97.93 |

a total of 12 rules. Although it is debatable, often designers use some cluster validity index to decide on the optimal number of rules (Bezdek & Pal, 1998; Pal et al., 2002). During rule refining some of the bad rules are pruned out and as a result the recognition score may be improved. But as we do not know the optimal number of rules for each class, it may be possible that our rule based system has missed some important rules. If that happens, some of the misclassified points should form clusters. Such misclassified points will share some common characteristics (we call such mistakes *typical mistakes*). In other words, if there are *subclusters* among the misclassified points, it is likely that some rules are missed by the rule extraction scheme. To fill this gap, a few extra rules, if required, are generated by analyzing the behavior of misclassifications (during training) made for a particular class. Possible clusters within the misclassified points are found by the *k*-means algorithm and each such cluster is converted into a fuzzy rule (as discussed in Section 2.3). These rules are added to the previous rule base which is then again tuned.

3. Data preparation

3.1. METEOSAT-5 imagery data

For the present study, we use the METEOSAT-5 VIS (0.5–0.9 μm) and IR (10.5–12.5 μm) images taken at 0500 UTC over the Indian subcontinent and in surrounding Indian Ocean (Fig. 1).

These high resolution raw METEOSAT-5 images are taken during the period 7th February–9th March 2003, a total of 31 days, and are provided by the European Organisation for the Exploration of Meteorological Satellites (EUMETSAT). The normal subsatellite resolutions for VIS and IR channels on the METEOSAT-5 images are 2.5 km and 5.0 km, respectively. All these images have a common center (over equator 63°E) and cover the same area. So an IR pixel corresponds to 4 VIS pixels. Since the VIS channel has the higher resolution, it contains more spatial details than the IR channel imageries. So we decided to apply the fuzzy rule base method at the resolution of VIS channel. To match the resolution of VIS image each IR pixel is divided into 4 pixels and all these 4 pixels are assumed to have the same brightness temperature of

Table 8
Confusion matrix on the training data over water

| Class | Cloudy | Partially cloudy | Clear sky |
|------------------|--------|------------------|-----------|
| Cloudy | 99.43 | 0.57 | 0.0 |
| Partially cloudy | 1.03 | 97.6 | 1.37 |
| Clear sky | 0.00 | 0.8 | 99.2 |

Table 9
Confusion matrix on the testing data over land

| Class | Cloudy | Partially cloudy | Clear sky |
|------------------|--------|------------------|-----------|
| Cloudy | 99.82 | 0.18 | 0.00 |
| Partially cloudy | 0.0 | 98.26 | 1.74 |
| Clear sky | 0.0 | 0.98 | 99.2 |

the original IR pixel. This allows us to use both the VIS and IR channels without losing any information.

The effects of solar illumination geometries on the VIS channel radiance (i.e., on VIS pixel value) is reduced using a standard Lambertian correction model, i.e., dividing all VIS pixel count by cosine of the solar zenith angle. The IR count is converted to brightness temperatures using the coefficients stored in the calibration block of the image header. Hereafter, VIS data will refer to corrected VIS image and IR data will refer to brightness temperature computed from IR gray level.

3.2. Computing the cloud-free background for visible channel images

Clouds are assumed to perturb the clear sky radiance (Connell et al., 2001; Kidder & Velder Haar, 1995; Reinke et al., 1992). A set of 31 images, each taken at 0500 UTC on 31 consecutive days, is analyzed to select the second darkest gray value to generate a background image for that particular hour.

The assumption is that dark pixels will not contain aerosols or clouds which would increase the reflectivity. We select the second darkest gray value for computing the composite clear sky background image. This will reduce the effect of possible contaminations by cloud shadows, highly dense pollutants, etc., which can cause a reduction in the satellite detected reflectivity. Except in very unusual situations, for any region we are not likely to have cloudy or snow-covered images for the entire period. Consequently, the background image thus produced will represent a clear sky condition with a high confidence. Any image acquisition system is subject to different types of uncertainty. Moreover, there are random variations in environmental conditions. So, it is quite possible that this background image may contain some noise. We use the median filter to reduce such noises in the background image. The mean difference from cloud-free background calculated using a 3×3 window around each pixel is used as a feature.

3.3. Creating the training and test data

To generate the data, we used a PC based image processing (IP) software for labeling of pixels. Since accurate labeling is the key to accurate classification, it is important to provide the analyst

Table 10
Confusion matrix on the testing data over water

| Class | Cloudy | Partially cloudy | Clear sky |
|------------------|--------|------------------|-----------|
| Cloudy | 99.27 | 0.73 | 0.0 |
| Partially cloudy | 0.89 | 97.67 | 1.44 |
| Clear sky | 0.00 | 0.25 | 99.75 |

Table 11
Ambiguous decisions during training and testing

| Firing strength threshold | Class no. ^a | Ambiguous decision (%) | | | | | | | |
|---------------------------|------------------------|------------------------|-------------------|------------------------|-------------------|------------------------|-------------------|------------------------|-------------------|
| | | Over land | | | | Over water | | | |
| | | Training | | Testing | | Training | | Testing | |
| | | Correct classification | Misclassification | Correct classification | Misclassification | Correct classification | Misclassification | Correct classification | Misclassification |
| α_{thres} | 1 | 0.03 | 0.00 | 0.02 | 0.00 | 0.03 | 0.00 | 0.06 | 0.00 |
| | 2 | 0.00 | 0.00 | 0.00 | 0.00 | 0.00 | 0.00 | 0.00 | 0.00 |
| | 3 | 0.00 | 0.00 | 0.00 | 0.00 | 0.00 | 0.00 | 0.00 | 0.00 |

^a 1=Cloudy, 2=partially cloudy, and 3=clear sky.

(meteorologist) with as much information as possible. A series of inbuilt image-processing functions are available to the analyst. For enhancement of the visual quality, images are histogram equalized. Since it is very easy to make labeling error, in particular, while labeling partially cloudy pixels, we took special care to examine wide variety of information before labeling.

This is a three-class problem. The selection of areas representing the two extreme classes, cloudy and clear sky, is not difficult. We have selected samples from those regions where there is no ambiguity, i.e., we have high confidence about whether it is cloudy or clear sky. The third class, partially cloudy, is comparatively difficult to label; in particular, when it is over the land. Mean brightness of partially cloudy pixels lie in between that of cloudy and clear sky. We choose samples for the partially cloudy class from those regions where we are sure about the fact that it is neither clear nor cloudy (e.g., thin cloud at the edge of a cloud deck, etc.). To be more accurate, a lower cut off, P_{low} , from clear sky and an upper level cut off, P_{up} , from cloudy region are defined as follows:

$$P_{\text{up}} = P_C - \sigma_C$$

$$P_{\text{low}} = P_{\text{NC}} + \sigma_{\text{NC}}$$

Here P_C and P_{NC} are the mean brightness of cloudy and clear sky regions, while σ_C and σ_{NC} are the corresponding standard

deviations for these classes. σ_C is almost the same over land and water surfaces, but σ_{NC} is low over water and high over land. We have considered only those areas which visually appear as partially cloudy and where pixels lie within the range defined by P_{up} and P_{low} .

Out of 31 images we select only one image (Fig. 2(a)) where the three classes appear distinctly. Some areas of this image are labeled for each of the three classes. As the radiative properties of land and water surfaces are distinctly different from each other, two separate rule based systems are designed for land and water, respectively, i.e., the labeled data are separated for land and water, respectively. Labeled samples contain a wide variety of cloudy, partially cloudy, and clear sky conditions over both the land and the ocean (Fig. 2(b)). The labeled data are summarized in Table 1.

A small percentage of the labeled data is randomly selected from each of the three classes over land and water to constitute the training data set. The remaining data constitute the test set. Let X be the entire data set, $X^l \cup X^w = X$. Here X^l and X^w are the data sets corresponding to land (l) and water (w), respectively. Now each of X^l and X^w is divided into training and test partition as $X_{\text{tr}}^* \cup X_{\text{te}}^* = X$, $X_{\text{tr}}^* \cap X_{\text{te}}^* = \Phi$, * corresponds to either l or w, X_{tr}^* and X_{te}^* are the training and test sets. Note that while applying the classifier using the latitude–

Table 12
Refined fuzzy rule base after adding extra rules for land surface

| Class | Rule no. | Feature no. | | | | | | | | | |
|------------------|----------|-------------|--------|----------|--------|----------|--------|----------|--------|----------|--------|
| | | 1 | | 2 | | 3 | | 4 | | 5 | |
| | | Centroid | Spread | Centroid | Spread | Centroid | Spread | Centroid | Spread | Centroid | Spread |
| Cloudy | 1 | 174.73 | 16.15 | 4.94 | 8.31 | 123.37 | 16.27 | 225.63 | 15.01 | 1.63 | 5.53 |
| | 2 | 150.12 | 14.48 | 10.17 | 10.64 | 112.10 | 14.62 | 263.22 | 15.06 | 0.91 | 4.07 |
| | 3 | 143.24 | 10.56 | 2.20 | 5.35 | 72.01 | 11.37 | 268.68 | 5.33 | 0.28 | 1.94 |
| | 4 | 123.75 | 14.61 | 12.64 | 11.58 | 86.57 | 14.17 | 266.66 | 13.51 | 1.32 | 4.69 |
| | 5 | 175.87 | 15.05 | 6.90 | 8.82 | 138.48 | 15.80 | 259.53 | 12.60 | 0.73 | 3.51 |
| Partially cloudy | 6 | 66.49 | 14.59 | 9.83 | 11.75 | 25.37 | 13.58 | 266.24 | 13.71 | 2.94 | 7.27 |
| | 7 | 83.19 | 12.99 | 6.09 | 10.11 | 27.46 | 14.08 | 254.68 | 15.97 | 2.37 | 7.09 |
| | 8 | 52.95 | 11.76 | 7.36 | 10.51 | 16.78 | 9.99 | 277.40 | 12.91 | 2.66 | 7.33 |
| Clear sky | 9 | 54.44 | 7.51 | 3.14 | 5.07 | 16.26 | 6.17 | 293.19 | 7.34 | 0.35 | 2.53 |
| | 10 | 63.96 | 16.53 | 1.00 | 4.40 | 6.06 | 13.49 | 287.37 | 16.48 | 0.22 | 0.98 |
| | 11 | 38.07 | 7.63 | 0.97 | 3.77 | 1.42 | 5.03 | 298.16 | 9.44 | 0.39 | 2.90 |
| | 12 | 85.53 | 9.27 | 2.17 | 4.32 | 22.33 | 8.28 | 279.09 | 5.67 | 0.45 | 2.07 |
| | 13 | 73.43 | 4.30 | 4.91 | 2.41 | 17.36 | 3.10 | 276.89 | 2.18 | 0.28 | 0.75 |
| | 14 | 51.93 | 2.68 | 1.42 | 1.04 | 12.28 | 1.47 | 293.15 | 2.88 | 0.60 | 0.40 |

Table 13
Classification results over land after adding extra rules

| Class | Correct classification (%) | |
|------------------|----------------------------|---------|
| | Training | Testing |
| Cloudy | 99.73 | 99.8 |
| Partially cloudy | 98.43 | 98.28 |
| Clear sky | 98.5 | 99.06 |
| Overall | 98.88 | 99.04 |

longitude information we can easily find whether the pixels are over land or water.

4. Classification results

For the present study we used 3000 randomly selected pixels from each class to generate the training set. Two such training–test partitions are prepared for each of land and water.

For both land and water portions of the image we used 5 features (i.e., $p=5$) and generated 5 rules for cloudy class, 4 rules for partially cloudy class, and 3 rules for clear sky class. The initial fuzzy rules are summarized in Table 2 (for land surface) and Table 3 (for water surface). As an illustration, in Table 4 we show the refined rule base for land. The pruning phase could not remove any rule. Comparison of the initial rules in Table 2 with the refined rules base in Table 4 shows that refinement makes noticeable changes in the rules. The initial centroids do not change much indicating that the clustering algorithm places the centroids in the right places. But the refinement algorithm makes significant changes in the spreads to reduce the training error. Similar changes are observed in the refined rule base for water also.

The classification results on the training and test data are summarized in Tables 5 and 6 for land and water, respectively. Table 5 shows that both training and test accuracies of classification over land for the cloudy pixels are very high (98–99%). The recognition score for partially cloudy is about 98%, while for the clear sky both the training and test accuracies are about 97% and 99%, respectively. The overall accuracy over land is about 98%. Similarly, over the ocean portion of the image, during refinement, none of the rules are pruned out. Table 6 shows that both training and test accuracies of classification for all three classes over water are also very high (97–99%). The overall accuracy is also about 98%. Another interesting observation is that for both land and water surfaces, the performance of the rule base on the training and test data is very consistent. The conclusion derived for the first training–test partition remains more or less the same for the second partition. This establishes the consistency and reliability of the proposed design methodology. The confusion matrices

Table 14
Confusion matrix on the training data over land after adding extra rules

| Class | Cloudy | Partially cloudy | Clear sky |
|------------------|--------|------------------|-----------|
| Cloudy | 99.73 | 0.27 | 0.0 |
| Partially cloudy | 0.00 | 98.43 | 1.57 |
| Clear sky | 0.0 | 1.5 | 98.5 |

Table 15
Classification results over water after adding extra rules

| Class | Correct classification (%) | |
|------------------|----------------------------|---------|
| | Training | Testing |
| Cloudy | 99.2 | 99.07 |
| Partially cloudy | 98.93 | 98.63 |
| Clear sky | 99.36 | 99.78 |
| Overall | 99.17 | 99.16 |

for training data are shown in Tables 7 and 8 for land and water, respectively.

Most of the misclassifications over land is made by the rules for the partially cloudy group: 0.27% cloudy pixels are being misclassified as partially cloudy whereas 2.07% clear sky cases are treated as partially cloudy. For cloudy and clear sky classes we have very few misclassifications. In 1.7% cases partially cloudy pixels are misclassified as clear sky (Table 7). Over water, the correct classification rate is very high: partially cloudy pixels are misclassified as cloudy and clear sky only in 1.03% and 1.37% cases, respectively; whereas 0.57% cloudy cases and 0.8% clear sky cases are being treated as partially cloudy (Table 8). Interestingly, over both land and water no cloudy pixel is misclassified as clear sky or vice versa; all misclassifications are limited to either the pair cloudy and partially cloudy or partially and clear sky (Tables 7 and 8). The confusion matrices over the test data exhibit the same pattern as that of the training data (Tables 9 and 10). This demonstrates the consistency of the rules extracted by our system.

Next we analyze the ambiguous or weak decisions. As explained in Section 2.5, we use the threshold, α_{thres} , for deciding on weak or ambiguous decision. An ambiguous decision may be correct or wrong. Table 11 summarizes the percentage of ambiguous decisions that are correct and wrong. Both over land and water the overall percentage of ambiguous decisions is very low. Over land, for class 1 only 0.02% decisions on the test data are ambiguous and all of them are correct. Similarly, over water only 0.06% decisions on the test data are ambiguous and all are correct decisions. For the other two classes practically, there is no ambiguous decisions. Thus, Table 11 reveals that both for land and water no ambiguous decision is misclassified. The observation also suggests that weak (ambiguous) decisions happen very rarely. However, this information on cloud will be very useful in detecting clouds over complex regions (e.g., sunglint region, snow-covered Himalayan region—such regions were not included in the data discussed above), which will be discussed later in Section 5.

We now add a few extra rules to model typical misclassifications as discussed in Section 2.6. During training,

Table 16
Confusion matrix on the training data over water after adding extra rules

| Class | Cloudy | Partially cloudy | Clear sky |
|------------------|--------|------------------|-----------|
| Cloudy | 99.2 | 0.8 | 0.0 |
| Partially cloudy | 0.33 | 98.93 | 0.74 |
| Clear sky | 0.0 | 0.64 | 99.36 |

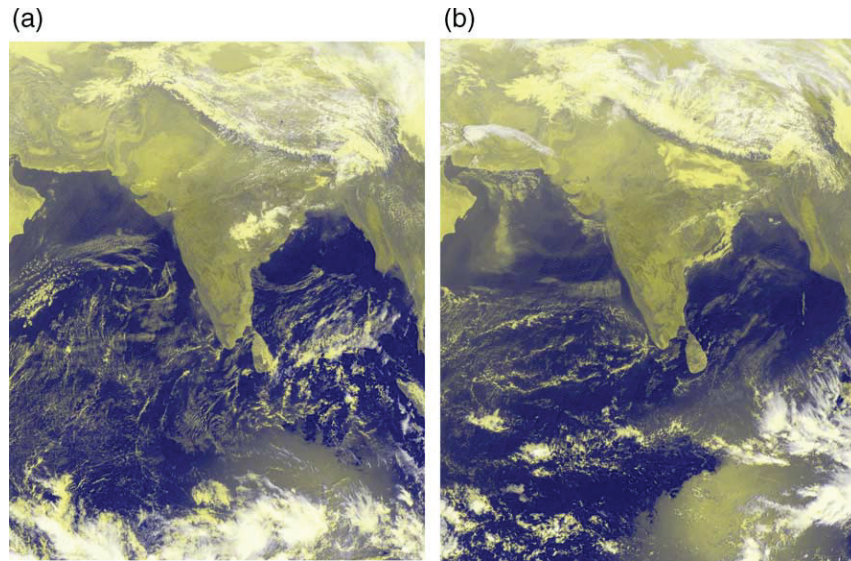


Fig. 3. False color images combining VIS and IR channels data (©2003 EUMET-SAT); (a) 0500 UTC 9th February 2003 and (b) 0500 UTC 20th February 2003.

in 2.07% cases, clear sky pixels over land are misclassified as partially cloudy (Table 7). Two extra rules are generated analyzing these misclassifications, which are then added to the previous rule base. Thus, the rule base now contains 5 rules from cloudy class, 4 from partially cloudy, and 5 (3+2) from the clear sky class. The extended rule base after refinement is given in Table 12. Inspection of Table 12 shows that for each of the new rules (rules 13 and 14) the spread of each membership function is much smaller than the corresponding spreads of other rules. Thus, these new rules have higher specificity and do not interfere with other rules which is revealed by the fact that inclusion of these new rules does not cause much changes to the performance of other rules (Table 12).

The classification results and confusion matrix obtained during training over land are summarized in Tables 13 and 14, respectively. The enhanced rule base shows a considerable improvement in classification result; particularly for clear sky class. For the clear sky class the percentage of correct classification is increased from 97.93% to 98.5% (Tables 5 and 13).

For the rule base corresponding to the areas over water again two rules are generated analyzing the misclassifications for partially cloudy class. Thus, the rule base now contains 5 rules from cloudy class, 6 (4+2) from partially cloudy, and 3 from clear sky class. The basic characteristics of the new rules are similar to rules 13 and 14 in Table 12. In other words, these new rules have higher specificity and do not interfere much

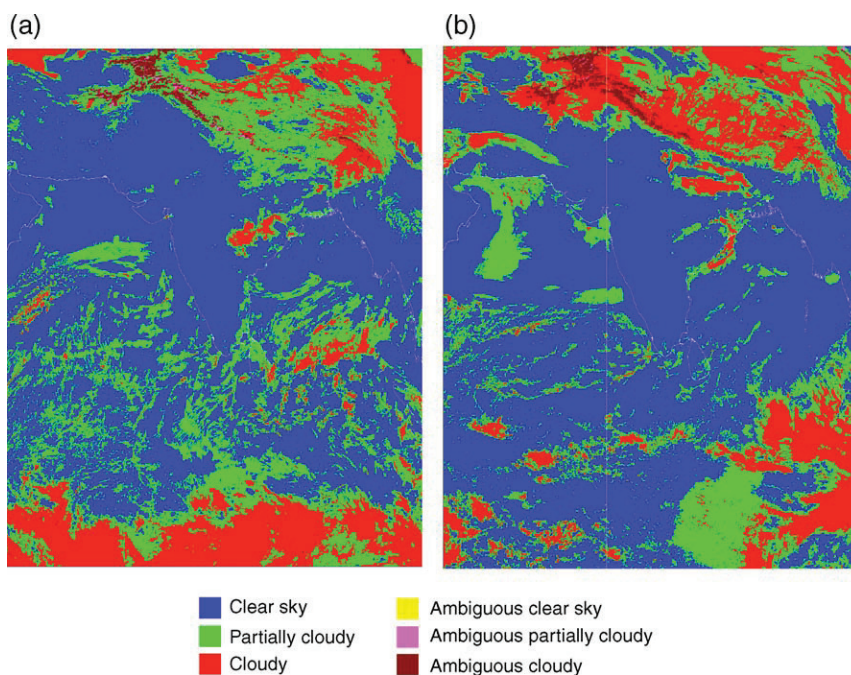


Fig. 4. Classification results without post-processing; (a) 0500 UTC 9th February 2003 and (b) 0500 UTC 20th February 2003.

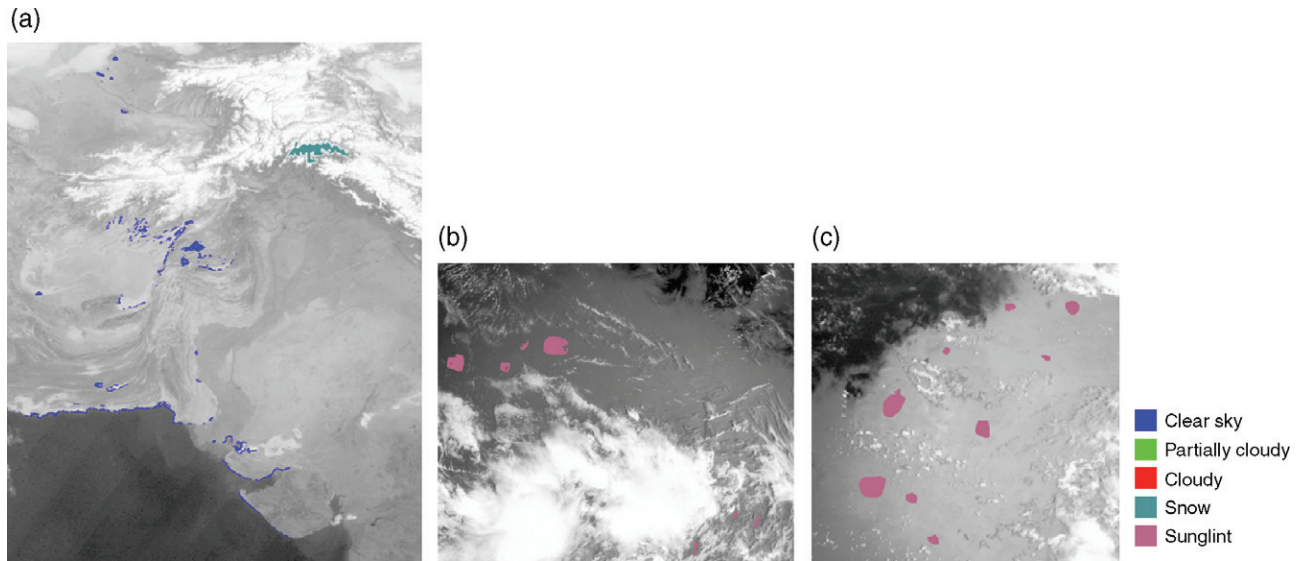


Fig. 5. Label data used in post-processing scheme; (a) samples of clear sky and snow classes, 0500 UTC 9th February 2003, (b) samples of sunglint class, 0500 UTC 9th February 2003, and (c) samples of sunglint class, 0500 UTC 20th February 2003.

with other rules. The classification results and confusion matrix obtained during training over water are summarized in Tables 15 and 16, respectively.

For a visual assessment of the results a set of false color images (combining VIS and IR data) for the dates 9th and 20th February 2003 are shown in Fig. 3, while Fig. 4 shows the corresponding classified images.

Note that, we have used only a part of the image taken on 9th February 2003 (Fig. 3(a)) for designing the rule base and tested it with images taken on the same as well as other dates (here 20th February 2003 (Fig. 3(b))). *A careful analysis of the classified images by domain experts reveals that most of the ambiguous and wrong decisions correspond to snow-covered Himalayan region or near to the sunglint region, and few of them also belong to coastline (Fig. 4(a) and (b)).* To overcome these problems we propose a post-processing scheme as discussed in the next section.

5. Post-processing

5.1. Post-processing scheme

Although the classifier works nicely over most part of the images, there are few regions where the partially cloudy class is

Table 17
Distribution of additional data points over land and water labeled by experts for post-processing

| Class | No. of pixels | |
|------------------|---------------|------------|
| | Over land | Over water |
| Cloudy | 0 | 0 |
| Partially cloudy | 0 | 0 |
| Clear sky | 2170 | 725 |
| Snow | 1115 | – |
| Sunglint | – | 6147 |
| Total | 3285 | 6872 |

being overestimated. This mostly happens over the region near the land–water boundary (e.g., coastal region or small water body within land) or at the boundary of different types of land cover where there is a high gradient in VIS/IR image. It also happens for the sunglint region where the mean VIS pixel intensity is quite higher than that of the normal clear sky region over water surface. Besides these, the snow-covered Himalayan region is mostly treated as ambiguous cloudy or ambiguous partially cloudy or sometimes wrongly classified (“false firing”) as cloudy or partially cloudy. The possible reasons for these “false firing” may be the ineffectiveness of the used features/data for some areas (e.g., VIS data within sunglint region) or the lack of representative samples in the training data (e.g., lack of samples from the coastal region and snow-covered Himalayan region). To overcome these problems, a post-processing scheme is proposed. The basic goal of this additional step is to reduce the “false firing” over several complex regions, specially at the boundaries of different land covers and coastal region, sunglint over water, and snow-covered mountain region.

During the post-processing of the classified image(s) experts detect some misclassified areas and label them for their correct class(es). Some of the “false firing” at the boundaries of different land covers and coastal region on the classified image(s) are labeled as clear sky class. Over the sunglint region, the problem is quite complicated. Due to specular reflections a large portion in this region is wrongly classified as partially cloudy when actually this region contains the sunglint pixels. To discriminate the partially cloudy pixels from the sunglint pixels a separate class named “sunglint” is added to the previous rule base for water surface. Domain experts label sunglint pixels within an approximate boundary of the sunglint region on the classified image(s). The approximate location of the sunglint region on the satellite image is found out with the scheme suggested by Giglio et al. (2003). It uses the angle θ_g between the vector pointing the

Table 18
Refined fuzzy rule base after post-processing for land surface

| Class | Rule no. | Feature no. | | | | | | | | | |
|------------------|----------|-------------|--------|----------|--------|----------|--------|----------|--------|----------|--------|
| | | 1 | | 2 | | 3 | | 4 | | 5 | |
| | | Centroid | Spread | Centroid | Spread | Centroid | Spread | Centroid | Spread | Centroid | Spread |
| Cloudy | 1 | 173.33 | 21.55 | 5.06 | 10.99 | 121.78 | 21.66 | 226.77 | 20.07 | 1.64 | 7.15 |
| | 2 | 149.84 | 17.83 | 10.59 | 13.65 | 111.88 | 17.99 | 263.18 | 17.29 | 0.98 | 5.32 |
| | 3 | 142.71 | 12.88 | 2.24 | 6.68 | 71.28 | 14.34 | 268.54 | 6.37 | 0.28 | 2.35 |
| | 4 | 122.43 | 18.67 | 12.97 | 15.04 | 85.19 | 18.24 | 265.93 | 17.17 | 1.46 | 6.29 |
| | 5 | 176.61 | 18.35 | 7.27 | 11.61 | 139.07 | 19.31 | 259.13 | 15.52 | 0.77 | 4.53 |
| Partially cloudy | 6 | 63.07 | 18.12 | 10.81 | 14.77 | 26.24 | 15.79 | 266.45 | 16.80 | 3.34 | 9.05 |
| | 7 | 81.82 | 17.75 | 6.55 | 13.55 | 27.45 | 18.98 | 254.68 | 19.99 | 2.53 | 9.24 |
| | 8 | 51.12 | 12.02 | 7.24 | 11.58 | 16.13 | 8.16 | 278.75 | 14.69 | 3.13 | 8.01 |
| | 9 | 54.41 | 8.45 | 3.14 | 6.09 | 16.60 | 6.69 | 293.53 | 7.20 | 0.27 | 1.80 |
| Clear sky | 10 | 64.54 | 19.45 | 1.20 | 8.15 | 6.30 | 16.57 | 285.84 | 20.87 | 0.24 | 0.91 |
| | 11 | 38.08 | 8.99 | 0.98 | 4.51 | 1.45 | 5.98 | 297.98 | 11.62 | 0.39 | 3.42 |
| | 12 | 86.24 | 11.31 | 2.05 | 5.24 | 22.69 | 10.17 | 279.28 | 6.94 | 0.44 | 2.33 |
| | 13 | 74.06 | 4.75 | 2.33 | 3.55 | 19.62 | 3.97 | 275.65 | 3.04 | 0.45 | 1.60 |
| | 14 | 51.26 | 2.86 | 1.10 | 1.69 | 11.61 | 2.09 | 293.44 | 3.11 | 0.72 | 0.96 |
| | 15 | 54.68 | 7.19 | 8.97 | 4.31 | 3.70 | 4.13 | 275.49 | 3.18 | 0.37 | 1.42 |
| | 16 | 64.37 | 5.11 | 6.18 | 3.85 | 11.88 | 4.42 | 277.70 | 3.28 | 0.52 | 1.14 |
| | 17 | 54.18 | 7.65 | 9.11 | 5.63 | 6.07 | 5.30 | 289.83 | 3.80 | 0.79 | 1.95 |
| | 18 | 76.81 | 7.64 | 6.97 | 5.18 | 16.87 | 6.79 | 278.74 | 6.28 | 0.34 | 1.61 |
| Snow | 19 | 168.35 | 14.39 | 22.76 | 8.34 | 22.12 | 13.11 | 255.24 | 4.05 | 1.32 | 2.19 |
| | 20 | 197.75 | 10.07 | 15.43 | 6.55 | 31.12 | 8.14 | 253.92 | 3.73 | 1.17 | 2.27 |

pixel-to-satellite direction and the specular reflection direction. The angle θ_g can be computed as

$$\cos\theta_g = \cos\theta_v \cos\theta_s - \sin\theta_v \sin\theta_s \cos\phi,$$

where θ_v and θ_s are the satellite view angle and solar zenith angle, respectively, and ϕ is the relative azimuth angle. The area defined by $\theta_g < 19^\circ$ over water is taken as the approximate boundary of the sunglint region. Similarly, over the snow-covered Himalayan region it is necessary to discriminate the cloudy/partially cloudy pixels from the snow-covered ones. Some of the ambiguous cloudy/partially cloudy and false firings over that region are labeled by the domain experts as a new class named “snow”.

These extra labeled data are divided into training–test data sets, and then some more fuzzy rules (as discussed in Section 2.3) are generated particularly for these problematic regions. The rules for coastal region (over land) and for boundaries of different land cover types are augmented to the clear sky class of the land module while the rules for “snow” are added as a new class (4th class) to the land module. Similarly, for the water module, the rules for coastal region (over water) are augmented to the clear sky class while the rules for “sunglint” are added as a new class (4th class) to the water module. The rules for the sunglint class are used only for the pixels within

the approximate boundary of sunglint region. The previous training–test data for both land and water surfaces are also augmented with these additional training–test data sets for the respective surfaces. Finally, the updated rule base for both land and water surfaces are tuned with respective updated training–test data sets. The classification results of post-processing are discussed in Section 5.2.

5.2. Results of post-processing

As discussed earlier, during post-processing of the classified image(s) some of the possible false fired regions are detected by experts and are labeled for their actual classes. The additional labeled samples are selected from the classified images taken on 9th and 20th February 2003 (Fig. 5).

The distribution of these additional data over different classes are shown in Table 17. For land and water surfaces the number of such labeled pixels are 3285 and 6872, respectively. For land surface, out of 3285 points only 650 pixels are randomly selected for training and the rest are treated as test data set. Four (4) rules for clear sky class and 2 rules for snow are generated using these 650 points and added to the previous rule base. The original training–test data are augmented using these additional data points and the entire data set is used in refining the updated rule base. The updated rule base now contains 5 rules for cloudy class, 4 rules for partially cloudy

Table 19
Classification results over land with updated rule base and labeled data

| Class | Correct classification (%) | |
|------------------|----------------------------|---------|
| | Training | Testing |
| Cloudy | 99.73 | 99.8 |
| Partially cloudy | 97.2 | 96.98 |
| Clear sky | 96.45 | 98.7 |
| Snow | 96.67 | 96.68 |
| Overall | 97.7 | 98.52 |

Table 20
Confusion matrix on the updated training data over land with updated rule base

| Class | Cloudy | Partially cloudy | Clear sky | Snow |
|------------------|--------|------------------|-----------|-------|
| Cloudy | 99.73 | 0.27 | 0.0 | 0.0 |
| Partially cloudy | 0.0 | 97.2 | 2.8 | 0.0 |
| Clear sky | 0.0 | 3.55 | 96.45 | 0.0 |
| Snow | 2.0 | 1.33 | 0.0 | 96.67 |

Table 21
Classification results over water with updated rule base and labeled data

| Class | Correct classification (%) | |
|------------------|----------------------------|---------|
| | Training | Testing |
| Cloudy | 99.27 | 99.11 |
| Partially cloudy | 98.6 | 98.4 |
| Clear sky | 99.32 | 99.82 |
| Sunglint | 94.53 | 94.31 |
| Overall | 98.77 | 98.99 |

class, 9 (3+2+4) rules for clear sky class, and 2 rules for snow class; Table 18. Comparing Table 18 with Table 12 we find that the new six rules do not alter much the description of the previous 14 rules. Unlike neural network type systems, this is a beauty of fuzzy rule base that it can be easily augmented by new rules. The classification results and the confusion matrix obtained on the training set over land are summarized in Tables 19 and 20, respectively. Similarly, for water surface 740 points are used for training and the rest are added to test set. This time only 1 rule is added to the clear sky class to eliminate the coastal false firings (similar to land surface post-processing) and 4 rules for the sunglint class are used to discriminate partially cloudy pixels from the sunglint pixels.

In this case also the new five rules do not change much of the 14 rules. For two rules, minor changes in the parameters are noticed, indicating that the average performance of the previous rule base will not change much. The classification results and the confusion matrix obtained on the training set over water are summarized in Tables 21 and 22, respectively.

Fig. 6 demonstrates the effectiveness of the post-processing scheme, on the images in Fig. 4 to account for the complex regions such as coastline, boundaries of different land covers, sunglint area over water, and snow-covered mountain region. The wrongly classified areas near the coastline and boundaries of different land covers are significantly reduced. The extra rules for sunglint further discriminate between partially cloudy and sunglint over sunglint region. Similarly, the additional rules for snow help to discriminate between cloudy/partially cloudy and snow over the snow-covered Himalayan region.

Comparison of the classification results before (Tables 13 and 15) and after the post-processing (Tables 19 and 21) shows that the extra rules added for clear sky class, sunglint, and snow during post-processing do not influence much the performance of the rules for the partially cloudy class (96.98–98.6%; Tables 13, 15, 19, and 21). The overall accuracy of the rules for clear sky is quite consistent over the water surface (99%; Tables 15 and 21), while over land surface it is reduced slightly (falls from 98.5% to 96.45%; Tables 13 and 19). Analysis of the performance of each rule for the clear sky class for land module reveals that during post-processing it exhibits a comparatively lower accuracy (84–88%) on the additional training–test data set of Table 17 than the initial rules (97–99%; Table 1). Besides these, rules for sunglint and snow have lower accuracy compared to other 3 classes (Tables 20 and 22). Consequently, the overall accuracy falls a little bit (Tables 13, 15, 19, and 21). These observations demonstrate that the post-processing primarily influences performances over those specific regions that

they are designed for and does not lead to any noticeable change on the performance of the previous rule base. This can also be seen from Fig. 6.

6. Comparisons

We have validated our method analyzing the results obtained on the test set. It shows a very high accuracy rate. However, there are other ways of validating these classification results. It is useful to see how they compare with the results of threshold techniques. It is also important to assess the validity of these results relative to conventional measurements or numerical model outputs. We discuss this next. A comparison with threshold techniques is presented in Section 6.1, and the possibility of verifications using other data is discussed in Section 6.2.

6.1. Comparison of classification results with multispectral threshold tests

To provide an alternative method of validation, the classification results on a test image taken at 0600 UTC, 1st March 2003 (Fig. 7(a) and (b)) are compared with those obtained from the multispectral threshold tests on the same image (Connell et al., 2001; Reinke et al., 1992; Rossow et al., 1985, 1996).

The threshold method classifies all image (VIS or IR) pixels as clear or cloudy according to whether the measured radiance differs from a reference “clear sky value” by more than a predefined “threshold value”. The clear sky and cloudy radiance are assumed to form a monotonic distribution with clear sky as an extremum (minimum brightness on the VIS image or maximum brightness temperature on the IR channel). The “clear sky value” for VIS channel is represented by the “cloud-free background” image (Section 3.2). Similarly, for the IR channel a maximum brightness temperature composite is computed by examining the 31 IR images taken during the period of our study. The threshold tests are performed using the VIS and IR channels individually as well as combining both of them together. The results are also compared with the International Satellite Cloud Climatology Project DX cloud data from METEOSAT-5 (ISCCP DX MET-5) (Rossow et al., 1996). Table 23 summarizes the different thresholds that are used and the corresponding results are shown in Figs. 8–10.

Comparison of the results of our classification scheme (Fig. 7(b)) and the multispectral threshold tests (Figs. 8–10) reveals the following:

- For VIS 10 count threshold (Fig. 8(a)) the cloud cover over water surface is underestimated, while over the land surface

Table 22
Confusion matrix on the updated training data over water with updated rule base

| Class | Cloudy | Partially cloudy | Clear sky | Sunglint |
|------------------|--------|------------------|-----------|----------|
| Cloudy | 99.27 | 0.73 | 0.0 | 0.0 |
| Partially cloudy | 0.53 | 98.6 | 0.63 | 0.24 |
| Clear sky | 0.03 | 0.55 | 99.32 | 0.01 |
| Sunglint | 0.0 | 5.47 | 0.0 | 94.53 |

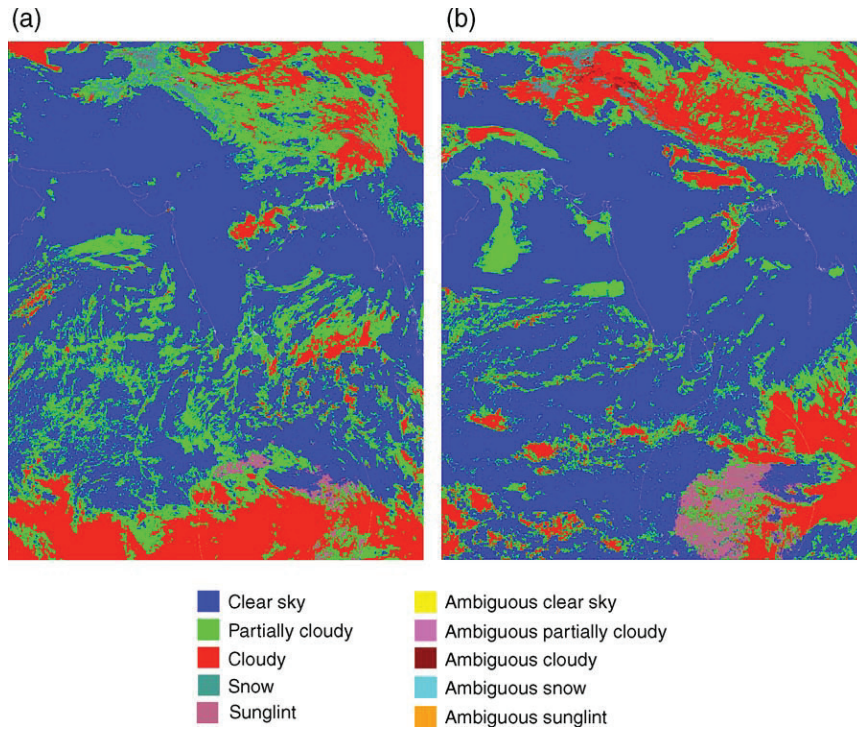


Fig. 6. Classified images after post-processing; (a) 0500 UTC 9th February 2003 and (b) 0500 UTC 20th February 2003. The approximate boundary of sunglint region is represented by the white curve drawn over the ocean portion of the classified images (near the lower right corner).

it is overestimated compared to our classification results. The sunglint region is overestimated with clouds, and the snow-covered Himalayan region is also treated as cloudy.

- For VIS 20 count threshold (Fig. 8(b)) the cloud cover, over both land and water surfaces, is underestimated

compared to our classification results. This threshold test fails to detect many low clouds and the thin cirrus clouds. The sunglint region is underestimated with clouds, and the snow-covered Himalayan region is mostly treated as cloudy.

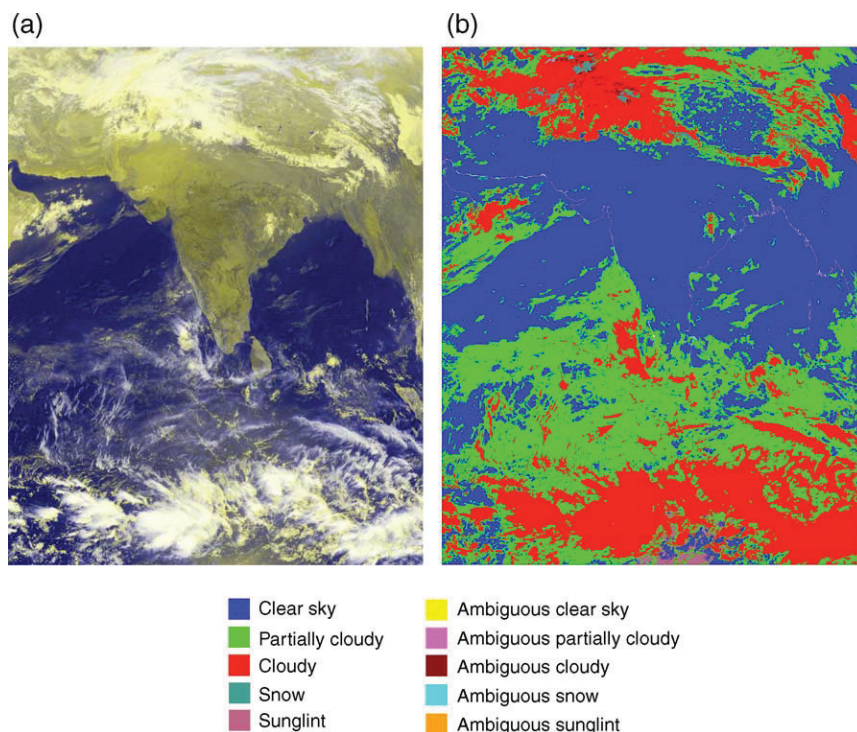


Fig. 7. Test image for comparison of classification results; (a) false color image combining VIS and IR channels data, 0600 UTC 1st March 2003 (©2003 EUMETSAT) and (b) classified image after post-processing, 0600 UTC 1st March 2003.

Table 23
Threshold tests

| Image/data | Threshold used |
|---------------------------|--|
| VIS | 10 VIS count (Reinke et al., 1992) 20 VIS count (Connell et al., 2001) |
| IR | 6 K brightness temperature (Rossow et al., 1985) 10 K brightness temperature (Connell et al., 2001) |
| VIS and IR combined | 10 VIS count and 6 K brightness temperature 10 VIS count and 10 K brightness temperature 20 VIS count and 6 K brightness temperature 20 VIS count and 10 K brightness temperature |
| ISCCP DX MET-5 cloud data | Bispectral threshold method (Rossow et al., 1996) |

- For IR 6 K threshold (Fig. 8(c)) the clear sky pixels over water are overestimated, while over the land surface it has resulted in a huge overestimation of clouds compared to our

classification results. Over the sunglint region the threshold test produces results that are, to some extent, comparable to our classification results. The snow-covered Himalayan region is mostly treated as cloudy.

- For IR 10 K threshold (Fig. 8(d)) the clouds over water are underestimated much more relative to our classification results. Over the sunglint region cloud cover is less compared to our results. Over the land surface, in general, this threshold produces an overestimation of clouds. Over the snow-covered Himalayan region clouds are underestimated.
- In general, for all the four VIS and IR combined thresholds (Fig. 9), there are underestimation of cloud cover over both land and water surfaces. The similar trend follows in the sunglint and the snow-covered Himalayan region (Figs. 7(b) and 9).

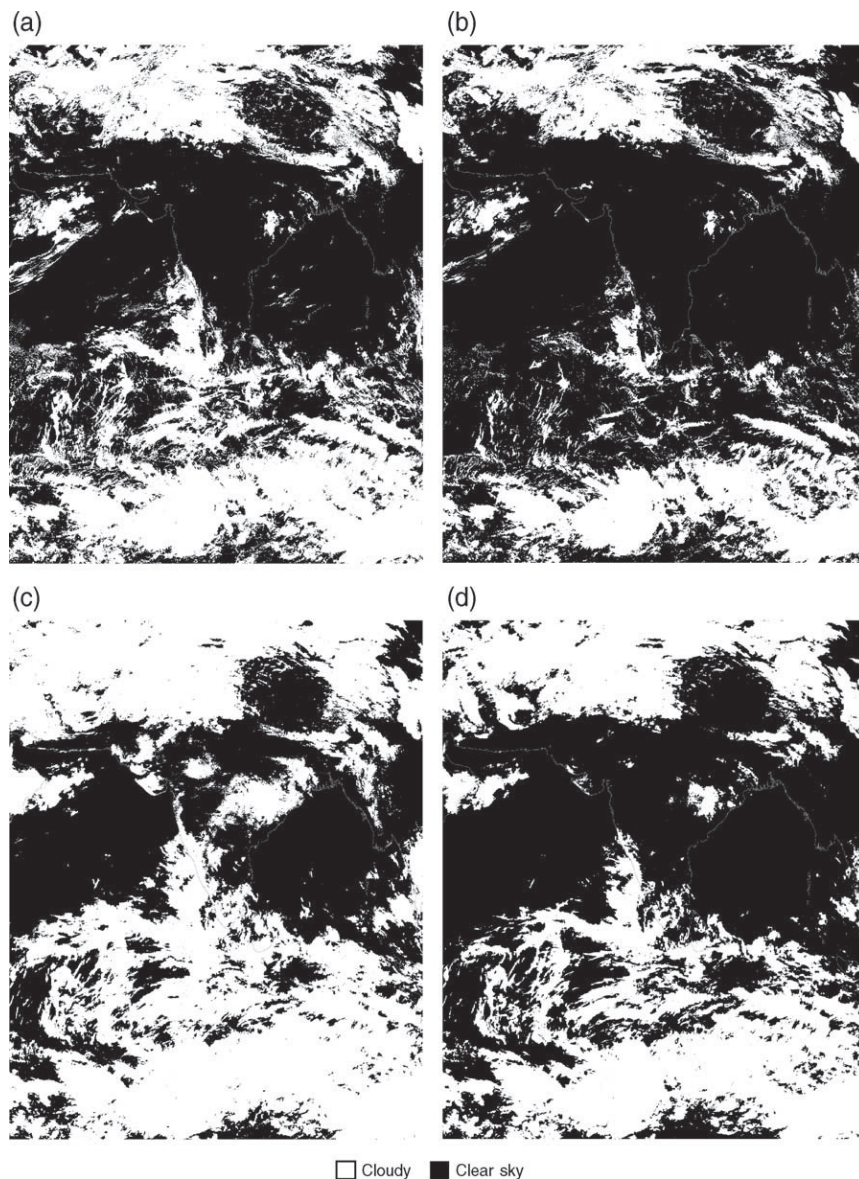


Fig. 8. Threshold tests on VIS and IR channels, 0600 UTC 1st March 2003; (a) VIS threshold 10 count, (b) VIS threshold 20 count, (c) IR threshold 6 K brightness temperature, and (d) IR threshold 10 K brightness temperature.

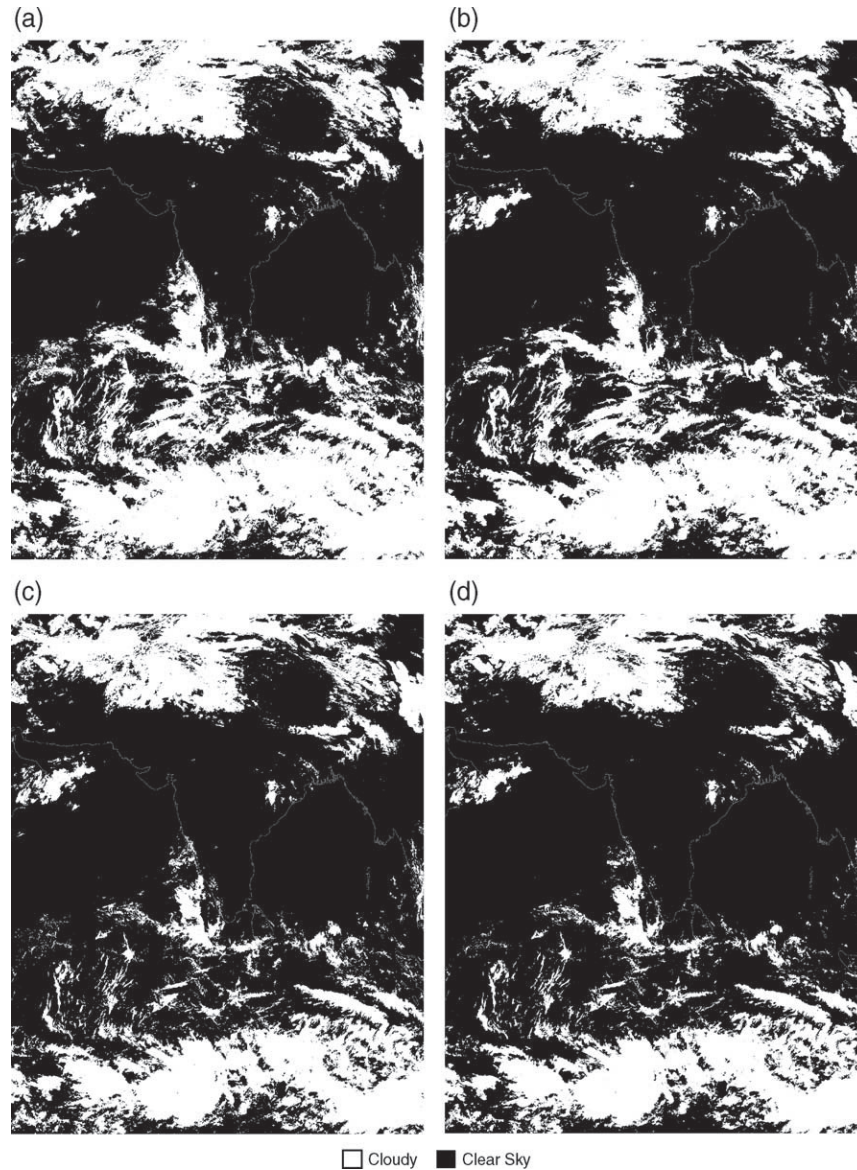


Fig. 9. Combined threshold tests on VIS and IR channels, 0600 UTC 1st March 2003; (a) VIS threshold 10 count and IR threshold 6 K brightness temperature, (b) VIS threshold 10 count and IR threshold 10 K brightness temperature, (c) VIS threshold 20 count and IR threshold 6 K brightness temperature, and (d) VIS threshold 20 count and IR threshold 10 K brightness temperature.

- Typically, for ISCCP DX MET-5 cloud data (Fig. 10) the overall pattern of cloud is quite similar to our classification results. However, ISCCP DX MET-5 data show an overestimation (underestimation) of clouds compared to our classification results over land (water). For both the land and water, the difference in cloud cover between ISCCP DX MET-5 data and our results is mainly due to the difference in detecting partially cloudy pixels. Within the sunglint region, in few cases, ISCCP DX MET-5 data overestimate the cloudy class. On the other hand, over the snow-covered Himalayan region, results are quite similar, and the “snow” pixels detected by our classifier mostly correspond to clear but snow flagged pixels of ISCCP DX MET-5 data.

It appears from the above comparison that the results of multispectral threshold tests are very much sensitive to the

thresholds used, and the situation becomes more complicated when there is a mixed/broken type of clouds (which we call partially cloudy). Consequently, the overestimation/underestimation of cloud results depends upon the thresholds. On the other hand, the proposed classification system extracts human interpretable linguistic rules for cloud cover estimation. The fuzzy rules can find the nonlinear class boundaries. This helps the classifier to accommodate partially cloudy pixels in a better way. Hence the threshold dependent underestimation/overestimation of cloudy pixels is reduced and the classifier shows an overall better performance compared to the multispectral threshold tests. Besides this, the critical analysis of errors, the ambiguity tests, and the post-processing scheme give the users some useful information as well as some interesting options to improve its performance further. Threshold tests do not provide such options to the users.

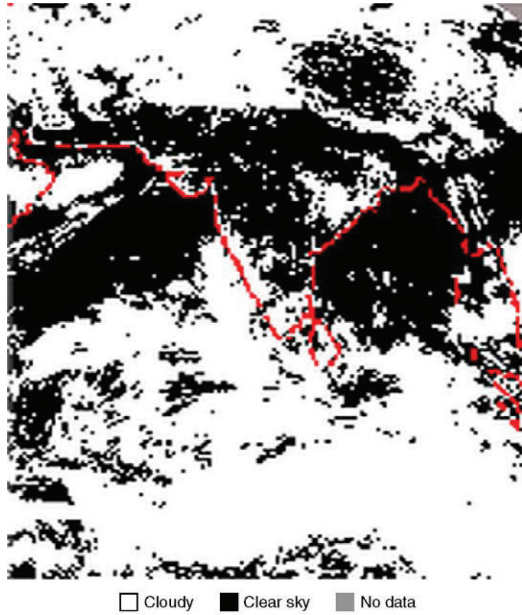


Fig. 10. ISCCP DX MET-5 cloud data, 0600 UTC 1st March 2003.

6.2. Comparison of classification results with synoptic surface observations and NCEP/NCAR reanalyzed total cloud cover data

6.2.1. Synoptic surface observations (SYNOP) data

Synoptic surface observations (SYNOP) are made by human experts at most operational weather stations. They provide an estimation of cloud cover in octas (unit of 1/8) and the type of the

most dominant cloud. Zero octa corresponds to a clear sky and eight octas corresponds to a completely overcast sky. These synoptic observations are estimated to be representative for an area with radius 20–30 km (Rossow et al., 1993).

To compare the classification results on the same test image in Fig. 7 with the SYNOP data on the same date and same time, we selected 11 surface stations in West Bengal and Tripura, India (shown in Fig. 11(a)). The SYNOP data for the 11 surface stations are provided by Regional Meteorological Center, India Meteorological Department, Calcutta, India. The circle in Fig. 11(b) covers an area of radius 25 km around each station, which approximately represents the field of view (FOV) of the observer.

The comparison is summarized in Table 24. The results indicate that almost all the cases which are detected as clear by the fuzzy rule based classifier correspond to low octa measurements (WMO station nos. 42811, 42503, 42403, 42206, and 42724) while the higher octa values (WMO station nos. 42807, 42809, 42707, 42708, and 42810) are associated with more number of cloudy and partially cloudy pixels detected within the circle of FOV. However, the agreement for the station 42901 is quite poor. So we can say that there is a general agreement between surface observations and satellite derived cloudiness. But, as indicated by Tuinder et al. (2004), it is very difficult to make general statements about the level of agreement between surface and satellite observations of cloud amount. The difficulties arise due to the completely different ways of observing the clouds: from above at a larger scale for the satellite, and from below with a restricted FOV for the ground observers. Taking into account these reasons, the

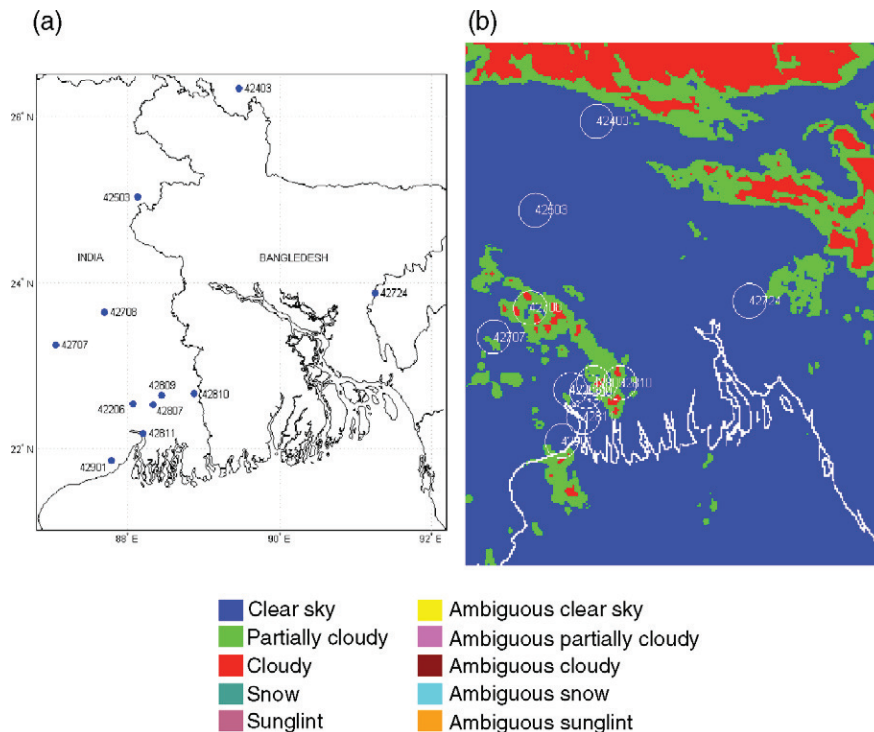


Fig. 11. Comparison with surface (SYNOP) observations; (a) location of surface stations denoted by ● and (b) surface stations with FOV circles on the classified image, 0600 UTC 1st March 2003.

Table 24
Comparison with surface observations (SYNOP)

| WMO station no. | Cloud cover | | | | |
|-----------------|-----------------------------|--|--------------------------------|---------------------|---------------------|
| | Ground observation in octas | Satellite observations within the circle of FOV (Fig. 11(b)) | | | |
| | | No. of cloudy pixels | No. of partially cloudy pixels | No. of clear pixels | Total no. of pixels |
| 42807 | 2 | 13 | 89 | 271 | 373 |
| 42809 | 3 | 15 | 193 | 165 | 373 |
| 42811 | 0 | 0 | 0 | 373 | 373 |
| 42503 | 0 | 0 | 0 | 373 | 373 |
| 42707 | 3 | 0 | 47 | 326 | 373 |
| 42708 | 4 | 55 | 254 | 59 | 373 |
| 42403 | 0 | 0 | 0 | 373 | 373 |
| 42206 | 0 | 0 | 24 | 349 | 373 |
| 42901 | 5 | 3 | 78 | 292 | 373 |
| 42724 | 0 | 0 | 3 | 370 | 373 |
| 42810 | 4 | 34 | 192 | 147 | 373 |

agreement between surface and satellite observations is considered to be reasonable.

6.2.2. NCEP/NCAR reanalyzed total cloud cover data

The NCEP/NCAR reanalyzed model data provide one of the best estimations of different meteorological parameters at a given instant of time over the globe (Kalnay et al., 1996) and these are being used by the meteorological community throughout the globe for initializing numerical models, proximity analysis for thunderstorms, climate studies, etc. (Brooks et al., 2003; Shea et al., 1994).

Here we also compare the classification results on the same test image in Fig. 7 with NCEP/NCAR reanalyzed total cloud cover (tcdc) data on the same date and time in a qualitative manner (Fig. 12).

The visual comparison shows that the gross pattern of distribution of clouds is quite similar. Most of the cloudy, partially cloudy, and clear regions in the classified image (Fig. 7(b)) correspond to high, medium, and low cloud covered (%) regions in the NCEP/NCAR tcdc data (Fig. 12), respectively. It only compares overall large-scale cloud structure in the classified satellite images. In case of the regions where the ground observations are hardly available, this comparison may be used as an alternative way of validation of the performance of the classifier. However, the resolution of NCEP/NCAR tcdc data is very low compared to that of the satellite images, and the detailed comparison at the lower scale is not possible.

7. Conclusions

We proposed a system for automatic extraction of human interpretable linguistic rules for cloud cover estimation with high accuracy. Unlike earlier attempts, which are mostly threshold based, it can find nonlinear class boundaries using fuzzy rules. It also can accommodate for partially cloudy areas, and hence, the threshold dependent overestimate/underestimate of cloudy pixels is reduced. Two separate classification

modules, one for land and one for water are derived primarily based on surface radiative properties. If the system makes similar mistakes repeatedly then new rules are added to model such typical mistakes. This is a very interesting property of the proposed system. The present study is limited to daytime analysis (as the VIS channel images are used) and no direct meteorological information is used except experts' (meteorologists) knowledge during labeling of the training data and post-processing of classified images.

The scheme is tested on images other than the training image(s). The performance of the system is found to be quite satisfactory; cloudy, partially cloudy, and clear sky over land and water are all classified with high accuracy.

However, the classifier initially could not produce very satisfactory results in detecting cloud over snow-covered surroundings or near the boundaries of different types of land cover. It also could not do a very good job on coast or shorelines, in areas with cloud shadows, and in extreme sunglint conditions. A post-processing scheme is then proposed which reduces the wrongly classified areas near the coastline, within sunglint area, and snow-covered Himalayan region quite effectively. Further, for the present study, we do not have information about aerosols, dust or smoke for the labeled data set. Dry aerosols may not create much of a problem. But the situation may become complicated when aerosols absorb moisture, start growing in size and finally form clouds.

If these swollen aerosols are present our classifier may treat them either partially cloudy or ambiguous partially cloudy or ambiguous cloudy depending upon its state of transition from aerosols to cloud formation. Similarly, dust or smoke may be classified as either clear sky or ambiguous clear sky or partially

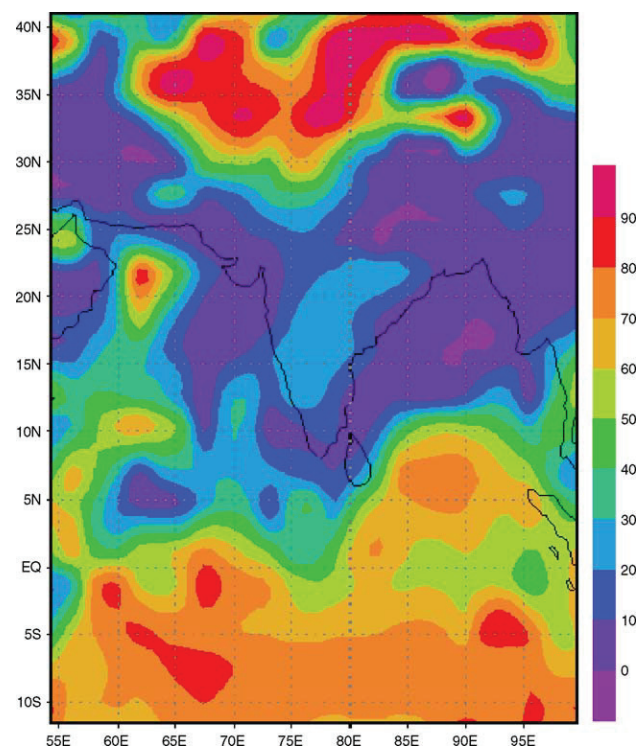


Fig. 12. NCEP/NCAR reanalyzed tcdc %, 0600 UTC 1st March 2003.

cloudy or ambiguous partially cloudy. In the future we plan to study the effect of aerosols, dust, smoke on the classifier. Investigation will also be carried out in identifying different types of clouds present within the cloudy and partially cloudy classes.

Acknowledgment

The first author acknowledges the Senior Research Fellowship of the Council of Scientific and Industrial Research (CSIR), India. Authors would also like to thank European Organisation for the Exploration of Meteorological Satellites (EUMETSAT) for providing the METEOSAT-5 data. The ISCCP DX data were obtained from the NASA Langley Research Center Atmospheric Sciences Data Center. The SYNOP data provided by Regional Meteorological Center, India Meteorological Department (Calcutta, India) are also acknowledged. NCEP Reanalysis data were provided by the NOAA-CIRES Climate Diagnostics Center, Boulder, Colorado, USA, from their web site at <http://www.cdc.noaa.gov/>. The anonymous referees deserve special thanks for providing very useful suggestions that have improved the manuscript.

Appendix A. The rule refinement algorithm

The tuning process is repeated until the rate of decrease in E becomes negligible. When product is used to compute the firing strength, the rule refinement algorithm is as follows:

Begin

Choose learning parameters η_m and η_s .

Choose a parameter reduction factor $0 < \varepsilon < 1$.

Choose the maximum number of iterations, maxiter .

Compute the error E_0 for the initial rule base R^0 .

Compute the misclassification M_0 corresponding to initial rule base R^0 .

$t \leftarrow 1$

While ($t \leq \text{maxiter}$) do

For each vector $\mathbf{x} \in X$

Find the rules R_c and R_{-c} .

Modify the parameters of rules and as follows.

For $k=1$ to p

$$\begin{aligned} v_{ck}^{\text{new}} &= v_{ck}^{\text{old}} - \eta_m \frac{\partial E}{\partial v_{ck}^{\text{old}}} \\ &= v_{ck}^{\text{old}} + \eta_m (1 - \alpha_c + \alpha_{-c}) \frac{\alpha_c}{\sigma_{ck}^{\text{old}}} (x_k - v_{ck}^{\text{old}}) \end{aligned}$$

$$\begin{aligned} v_{-ck}^{\text{new}} &= v_{-ck}^{\text{old}} - \eta_m \frac{\partial E}{\partial v_{-ck}^{\text{old}}} \\ &= v_{-ck}^{\text{old}} - \eta_m (1 - \alpha_c + \alpha_{-c}) \frac{\alpha_{-c}}{\sigma_{-ck}^{\text{old}}} (x_k - v_{-ck}^{\text{old}}) \end{aligned}$$

$$\sigma_{ck}^{\text{new}} = \sigma_{ck}^{\text{old}} - \eta_s \frac{\partial E}{\partial \sigma_{ck}^{\text{old}}}$$

$$= \sigma_{ck}^{\text{old}} + \eta_s (1 - \alpha_c + \alpha_{-c}) \frac{\alpha_c}{\sigma_{ck}^{\text{old}}} (x_k - v_{ck}^{\text{old}})^2$$

$$\sigma_{-ck}^{\text{new}} = \sigma_{-ck}^{\text{old}} - \eta_s \frac{\partial E}{\partial \sigma_{-ck}^{\text{old}}}$$

$$= \sigma_{-ck}^{\text{old}} - \eta_s (1 - \alpha_c + \alpha_{-c}) \frac{\alpha_{-c}}{\sigma_{-ck}^{\text{old}}} (x_k - v_{-ck}^{\text{old}})^2$$

End For

End For

Compute the error E_t for the new rule base R^t .

Compute the misclassification M_t for R^t .

If $M_t > M_{t-1}$ or $E_t > E_{t-1}$

then

$$\eta_m \leftarrow (1 - \varepsilon) \eta_m$$

$$\eta_s \leftarrow (1 - \varepsilon) \eta_s$$

$$R^t \leftarrow R^{t-1}$$

/* If the error is increased, then possibly the learning coefficients are too large. So, decrease the learning coefficients and restore the rule base to R^t . */

If $M_t = 0$ or $E_t = 0$

then Stop

$t \leftarrow t + 1$

End while

End

References

- Baum, B. A., et al. (1995). Satellite remote sensing of multiple cloud layers. *Journal of the Atmospheric Sciences*, 52, 4210–4230.
- Baum, B. A., Tovinkere, V., Titlow, J., & Welch, R. M. (1997). Automated cloud classification of global AVHRR data using a fuzzy logic approach. *Journal of Applied Meteorology*, 36, 1519–1540.
- Bezdek, J. C., & Pal, N. R. (1998). Some new indexes of cluster validity. *IEEE Transactions on Systems, Man, And Cybernetics*, 28, 301–315.
- Brooks, H. E., Lee, J. W., & Craven, J. P. (2003). The spatial distribution of severe thunderstorm and tornado environments from global reanalysis data. *Atmospheric Research*, 67–68, 73–94.
- Chiu, S. L. (1994). Fuzzy model identification based on cluster estimation. *Journal of Intelligent & Fuzzy Systems*, 2, 267–278.
- Coakley Jr., J. A., & Baldwin, D. G. (1984). Towards the objective analysis of clouds from satellite imagery data. *Journal of Climate and Applied Meteorology*, 23, 1065–1099.
- Coakley Jr., J. A., & Bretherton, F. P. (1982). Cloud cover from high-resolution scanner data: Detecting and allowing for partially filled fields of view. *Journal of Geophysical Research*, 87, 4917–4932.
- Connell, B. H., Gould, K. J., & Purdom, J. F. W. (2001). High-resolution GOES-8 visible and infrared cloud frequency composites over northern Florida during the summers 1996–99. *Weather and Forecasting*, 16, 713–724.
- Desbois, M., Seze, G., & Szejwach, G. (1981). Automatic classification of clouds on METEOSAT imagery: Application to high-level clouds. *Journal of Applied Meteorology*, 21, 401–412.
- Ebert, E. (1987). A pattern recognition technique for distinguishing surface and cloud types in the polar regions. *Journal of Climate and Applied Meteorology*, 26, 1412–1427.
- Ebert, E. (1989). Analysis of polar clouds from satellite imagery using pattern recognition and a statistical cloud analysis scheme. *Journal of Applied Meteorology*, 28, 382–399.
- Giglio, L., Descloitres, J., Justice, C. O., & Kaufman, Y. J. (2003). An enhanced contextual fire detection algorithm for MODIS. *Remote Sensing of Environment*, 87, 273–282.

- Goodman, A. H., & Henderson-Sellers, A. (1988). Cloud detection and analysis: A review of recent progress. *Atmospheric Research*, 21, 203–228.
- Hughes, N. A. (1984). Global cloud climatologies: A historical review. *Journal of Climate and Applied Meteorology*, 23, 724–751.
- Kalnay, E., Kanamitsu, M., Kistler, R., Collins, W., Deaven, D., Gandin, L., et al. (1996). The NCEP/NCAR 40-year reanalysis project. *Bulletin of the American Meteorological Society*, 77, 437–471.
- Key, J. R., Maslanik, J. A., & Barry, R. G. (1989). Cloud classification from satellite data using a fuzzy sets algorithm: A polar example. *International Journal of Remote Sensing*, 10, 1823–1842.
- Kidder, S. Q., & Velder Haar, T. H. (1995). *Satellite Meteorology: An Introduction* (pp. 259–290). New York: Academic Press.
- Klir, G. J., & Yuan, B. (2001). *Fuzzy sets and Fuzzy logic: Theory and Applications*. New Delhi: Printice-Hall of India Private Limited.
- Lee, J., Weger, R. C., Sengupta, S. K., & Welch, R. M. (1990). A neural network approach to cloud classification. *IEEE Transactions on Geoscience and Remote Sensing*, 28, 846–855.
- Norris, J. R. (2000). What can cloud observations tell us about climate variability? *Space Science Reviews*, 94, 375–380.
- Pairman, D., & Kittler, J. (1986). Clustering algorithms for use with images of clouds. *International Journal of Remote Sensing*, 7, 855–866.
- Pal, K., Mudi, R., & Pal, N. R. (2002). A new scheme for fuzzy rule based system identification and its application to self-tuning fuzzy controllers. *IEEE Transactions on Systems, Man and Cybernetics. Part B. Cybernetics*, 32, 470–482.
- Pankiewicz, G. S. (1995). Pattern recognition techniques for the identification of cloud and cloud systems. *Meteorological Applications*, 2, 257–271.
- Reinke, D. L., Combs, C. L., Kidder, S. Q., & Vonder Haar, T. H. (1992). Satellite cloud composite climatologies: A new high-resolution tool in atmospheric research and forecasting. *Bulletin of the American Meteorological Society*, 73, 278–285.
- Rossow, W. B. (1989). Measuring cloud properties from space: A review. *Journal of Climate*, 2, 201–213.
- Rossow, W. B., Mosher, F., Kinsella, E., Arking, A., Desbois, M., Harrison, E., et al. (1985). ISCCP cloud algorithm intercomparison. *Journal of Climate and Applied Meteorology*, 24, 877–903.
- Rossow, W. B., Walker, A. W., Beusichel, D. E., & Roiter, M. D. (1996). International Satellite Cloud Climatology Project (ISCCP) Documentation of New Cloud Datasets. WMO/TD-No. 737, World Meteorological Organization.
- Rossow, W. B., Walker, A. W., & Garder, L. C. (1993). Comparison of ISCCP and other cloud amounts. *Journal of Climate*, 6, 2394–2418.
- Seze, G., & Desbois, M. (1987). Cloud cover analysis from satellite imagery using spatial and temporal characteristics of the data. *Journal of Climate and Applied Meteorology*, 26, 287–303.
- Seze, G., & Pawloska, H. (2001). Cloud cover analysis with METEOSAT-5 during INDOEX. *Journal of Geophysical Research*, 106, 28415–28426.
- Shea, J. D., Steven, J. W., Stern, I. R., & Hoar, J. T. (1994). An Introduction to Atmospheric and Oceanographic Data. NCAR Technical Note (NCAR/TN-404+IA).
- Simmer, C., Raschke, E., & Ruprecht, E. (1982). A method for determination of cloud properties from two-dimensional histograms. *Annalen der Meteorologie*, 18, 130–132.
- Tovinkere, V. R., Penaloza, M., Logar, A., & Lee, J. (1993). An intercomparison of artificial intelligence approaches for polar scene identification. *Journal of Geophysical Research*, 98, 5001–5016.
- Tuinder, O. N. E., de Winter-Sorkina, R., & Bultjes, P. J. H. (2004). Retrieval methods of effective cloud cover from the GOME instrument: An intercomparison. *Atmospheric Chemistry and Physics*, 4, 255–273.
- Wielicki, B. A., Cess, R. D., King, M. D., Randall, D. A., & Harrison, E. F. (1995). Mission to Planet Earth: Role of clouds and radiation in climate. *Bulletin of the American Meteorological Society*, 76, 2125–2153.